1-1-2019

The Tara Pacific expedition—A pan-ecosystemic approach of the "-omics" complexity of coral reef holobionts across the Pacific Ocean

Serge Planes
École Pratique des Hautes Etudes

Denis Allemand
Centre Scientifique de Monaco

Sylvain Agostini
The Shimoda Marine Research Center

Bernard Banaigs
École Pratique des Hautes Etudes

Emilie Boissin
École Pratique des Hautes Etudes

See next page for additional authors

Research Article | Vol. 27, No. 21 / 14 October 2019 / Optics Express 30191
Optics EXPRESS

Evaluating satellite estimates of particulate backscatter in the global open ocean using autonomous profiling floats

K. M. Bisson,[1,*] E. Boss,[2] T. K. Westberry,[1] and M. J. Behrenfeld[1]

[1]Department of Botany and Plant Pathology, Oregon State University, Corvallis, Oregon 97331, USA
[2]School of Marine Sciences, University of Maine, Orono, Maine 04469, USA
[*]bissonk@oregonstate.edu

Abstract: Satellite retrievals of particulate backscattering (b_{bp}) are widely used in studies of ocean ecology and biogeochemistry, but have been historically difficult to validate due to the paucity of available ship-based comparative field measurements. Here we present a comparison of satellite and in situ b_{bp} using observations from autonomous floats (n = 2,486 total matchups across three satellites), which provide b_{bp} at 700 nm. With these data, we quantify how well the three inversion products currently distributed by NASA ocean color retrieve b_{bp}. We find that the median ratio of satellite derived b_{bp} to float b_{bp} ranges from 0.77 to 1.60 and Spearman's rank correlations vary from r = 0.06 to r = 0.79, depending on which algorithm and sensor is used. Model skill degrades with increased spatial variability in remote sensing reflectance, which suggests that more rigorous matchup criteria and factors contributing to sensor noisiness may be useful to address in future work, and/or that we have built in biases in the current widely distributed inversion algorithms.

1. Introduction

Satellite observations of particulate backscattering (b_{bp_sat}) have advanced our understanding of ocean biology over the last few decades by using b_{bp_sat} as a proxy for particulate organic carbon [1], phytoplankton biomass [2], and particle size [3]. There are three algorithms for which NASA's Ocean Biology Processing Group distributes b_{bp_sat} products. While they are widely used, it remains a challenge to compare satellite and in situ observations of b_{bp} at global scales. The extreme paucity of in situ data stands as a significant barrier to evaluating methods that retrieve b_{bp_sat}, and ultimately to understand how these biases may influence the application of b_{bp} for global questions. The ongoing deployment of worldwide autonomous floats equipped with backscattering sensors at 700 nm makes it possible to compare in situ b_{bp} from these platforms with algorithms for b_{bp_sat}.

Autonomous profiling floats (of the Bio-geochemical Argo program, [4]) have recently become the backbone of a global array for biogeochemical monitoring. These float measurements have since been used for a variety of applications [5–8], including regional assessments of ocean color products [9]. Floats supply a valuable source of data to assess satellite performance because they continuously monitor the global ocean in seasonally under sampled places infrequently accessed by ships. Floats spend most of their time in cold dark waters ~1000m deep, so biofouling and lateral drift are minimized [10], although they do occur, particularly in warm waters [11]. There is low individual probability for coincident measurements with satellites (due to cloud cover and seasonal darkness), but the sustained sampling and spatial coverage of float observations yields many more satellite matchups compared to ship-based observations of b_{bp}, especially in open ocean regions that are severely under sampled with respect to b_{bp}.

#370807 https://doi.org/10.1364/OE.27.030191
Journal © 2019 Received 2 Jul 2019; revised 16 Aug 2019; accepted 2 Sep 2019; published 4 Oct 2019

Optics EXPRESS

This study builds off of the success of previous work that has advanced our understanding of remote sensing inversion algorithms to predict in situ observations of b_{bp} [12,13]. Most of these studies have relied on a limited number of shipboard observations and/or simulated datasets for the remote sensing reflectance (R_{rs}) values used to derive b_{bp}. There exist more recent studies comparing R_{rs} - derived estimates of b_{bp} to in situ observations, but they do so at limited regional scales [9,14,15]. A broader understanding of how spaceborne estimates of particulate backscatter compare with globally distributed in situ observations is still needed. The aim of this study is to compare b_{bp} observations from floats (n = 2,486 surface matchups) and satellites in order to identify paths forward for improving b_{bp_sat} in the open ocean.

2. Data and methods

2.1. Bio-argo float data: acquisition and processing

Vertical profiles of b_{bp_float} (700 nm, m^{-1}) were acquired from the Argo Global Data Assembly Centre (GDAC) ftp site (ftp://ftp.ifremer.fr/ifremer/argo/etc/argo-synthetic-profile, on 30 January 2019, [16]), the Southern Ocean Carbon and Climate Modeling database (SOCCOM, on 14 January 2019), the NASA North Atlantic Aerosols and Marine Ecosystems project (NAAMES, http://misclab.umeoce.maine.edu/floats/, on 18 January 2019), and through the Monterey Bay Aquarium Research Institute (MBARI, https://www3.mbari.org/chemsensor/MBARI_float_table/mbari_float_table.html, on 8 Feb 2019). Float measurements of b_{bp} have a known uncertainty on the order of 10-15% [17]. Floats are not perfect platforms and they can be subject to instrumental drift and calibration issues arising from using only the manufacturer calibration file rather than performing sensor-specific calibrations with dark counts. In all cases, the quality-controlled (QC) data flagged as 'bad data' by the ARGO QC Data management team were removed [18], as well as additional outliers. Outliers were defined as b_{bp_float} values outside the bounds given by 1.5 times the interquartile range (+/− the 75th and 25th percentile, respectively) of log-transformed b_{bp_float} data. In total, 850 observations were removed, or approximately 2% of all observations. After outliers and bad data are removed, this data compilation consists of 37,165 independent lat/lon/time b_{bp} observed vertical profiles (700 nm, m^{-1}) at resolutions ranging from 0.5m to 5m depending on the location and dataset (Fig. 1).

Profiles of b_{bp_float} were processed to make them comparable with remote sensing reflectance products by computing the average b_{bp} in the surface mixed layer. Mixed layer depth (MLD) was calculated in each profile as the depth where density exceeds 0.03 kg m^{-3} relative to the density at 10 m [19]. Next, each vertical profile was de-spiked with a 3-point moving median within the MLD to remove the backscattering contribution of bubbles [20]. De-spiking the profiles reduced the median of all b_{bp_float} observations from 9.7×10^{-4} m^{-1} to 9.0×10^{-4} m^{-1} and it reduced (on average) the interquartile range within all profiles from $\sim 3 \times 10^{-4}$ m^{-1} to $\sim 1 \times 10^{-4}$ m^{-1}. Finally, we averaged the de-spiked b_{bp} values within the MLD for each float profile, assuming that MLD is equivalent to the active mixing depth. We note using a processing depth of the first light attenuation layer does not change the values of b_{bp_float} for the places and times used in this study.

2.2. Satellite data: acquisition and processing

Remote sensing reflectance (R_{rs}, sr^{-1}) data were acquired for MODIS (Moderate Resolution Imaging Spectroradiometer, nadir viewing resolution = 1 km), VIIRS (Visible Infrared Imaging Radiometer Suite, nadir viewing resolution = 750 m), and OLCI (the SENTINEL-3 Ocean and Land Colour Instrument, nadir viewing resolution = 1.2 km) sensors. MODIS and VIIRS Level-2 scenes were downloaded from the NASA ocean color website (https://oceandata.sci.gsfc.nasa.gov/) and OLCI Level-2 scenes were downloaded from EUMETSAT (https://codarep.eumetsat.int/). Specific ocean color scenes were identified for download if they coincided with a float observation

Optics EXPRESS

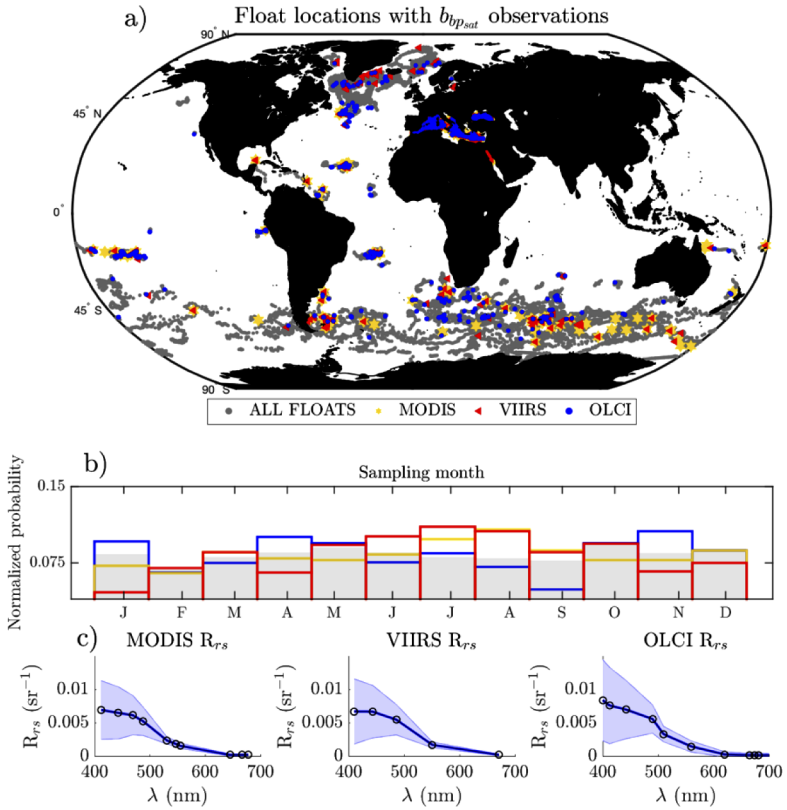

Fig. 1. a) A map of float observations used in this study, colored by matchups with a particular sensor. Grey represents float observations without coincident satellite matchups. b) Distribution of sampling month for all float observations and for those that coincide with a particular satellite sensor. c) Median (dotted line) and the interquartile range (blue shading) of satellite remote sensing reflectance for the matchup times and locations used in this study.

within a +/- 3 hour window. R_{rs} data were considered according to the matchup criteria in [21], hereafter referred to as the 'Bailey and Werdell criteria.' In particular, the solar zenith angle must be less than 75 degrees, at least half of the pixels in a 5×5 pixel box centered on the float location must be unflagged (unflagged data are free from failed atmospheric corrections, are not land pixels, etc.), and the median coefficient of variation for bands between 412 and 555 nm (and for the aerosol optical thickness at 865 nm) within the 5×5 box must be less than 15%. Remote sensing reflectances that meet these criteria are considered to be in spatially homogeneous waters that are roughly coincident with the timing of a float observation, and are minimally influenced by clouds, sun glint, and/or other atmospheric correction problems. Figure 1 shows where and when there are float-satellite match-ups that meet the Bailey and Werdell criteria (n = 539 matchups for MODIS, n = 840 matchups for VIIRS, n = 1107 matchups for OLCI). The spatial bias in the distribution of float observations with satellite matchups is substantial due, in part, to the geographical bias in float distribution.

All R_{rs} data were corrected to remove the contribution of Raman scattering Eqs. (1,2). Raman scattering is a spectrally continuous process whereby water molecules absorb photons and re-emit them at different wavelengths. If Raman scattering is unaccounted for, this can introduce bias into estimates of derived inherent optical properties, including b_{bp}, especially for wavelengths greater than 550 nm [22,23]. At the time of writing, the standard R_{rs} products distributed by

Optics EXPRESS

NASA (at all processing levels, from 1997 – present) are not corrected for Raman scattering. We note that the documented average difference between b_{bp_sat} derived from Raman corrected R_{rs} versus b_{bp_sat} that does not use Raman corrections has been shown to be as large as 20% for wavelengths between 412 and 670 nm [24].

There are both empirical and analytical approaches [15,23–27] to account for the Raman contribution to $R_{rs}(\lambda)$. Rather than investigate the differences in derived b_{bp_sat} from the choice of Raman scattering algorithm, in this study we apply the correction of [25] and use interpolated parameters to specific wavelengths when appropriate. We choose the algorithm in [25] because it has documented low uncertainty, the parameters it requires were derived over a realistic range of open ocean optical values, and it involves no additional data inputs (which would introduce an additional source of uncertainty, documented in [26]).

The Raman corrected R_{rs} is given by:

$$R_{rs} = \frac{R_{rs}^{T}}{1 + RF} \tag{1}$$

Where $R_{rs}{}^{T}$ is the R_{rs} from satellite observations, and RF, the 'Raman Factor,' is given by:

$$RF(\lambda) = a(\lambda)^{*} \left(\frac{R_{rs}^{T}(440)}{R_{rs}^{T}(550)}\right) + \beta_1(\lambda)^{*} R_{rs}^{T}(550)^{\beta_2(\lambda)} \tag{2}$$

Values of β_1, and β_2 were derived from Hydrolight simulations for chlorophyll values ranging from 0.02 to 3 μg L^{-1} and the reported model uncertainty is small (3%, [25]). We corrected R_{rs} from each sensor for all wavelengths between 410 and 700 nm so that they can be used in inversion algorithms to obtain b_{bp_sat}. The effect of Raman scattering is greatest at higher wavelengths. In this study, the median fraction of R_{rs} to $R_{rs}{}^{T}$ at 667 nm is 0.91 with an interquartile range of 0.04.

The retrieval of b_{bp_sat} is an inverse problem requiring a forward model that describes the relationship between R_{rs} and b_{bp_sat}. There are several published inversion algorithms available to determine b_{bp_sat}, and we consider the three model b_{bp_sat} products currently distributed by the NASA ocean color processing group: the Generalized Inherent Optical Property algorithm (GIOP, [28]), the Garver-Siegel-Maritorena algorithm (GSM, [29]), and the Quasi Analytical Algorithm (QAA, [30]). The goal of the GSM and GIOP inversion algorithms is to minimize the difference between modeled and observed R_{rs} using routine optimization techniques (see Appendix A for more details). The goal of the QAA is to analytically invert R_{rs} by first calculating the total absorption coefficient at a reference wavelength so that b_{bp_sat} can be algebraically determined using the inverted ratio of total backscattering to total absorption. In these algorithms, b_{bp_sat} is determined in combination with empirical coefficients for particulate absorption and absorption by colored dissolved and detrital material, which will both impact estimates of b_{bp_sat}. When in their default configuration, the general architecture of these three algorithms is similar but they differ in their assumptions of inherent optical property spectral shape and in their optimization techniques. Complete details are given in Appendix A.

In this study, we calculate b_{bp_sat} from the GIOP, QAA, and GSM algorithms for every location and time with a float matchup observation. Observations of b_{bp_sat} are extrapolated to 700 nm for direct comparison to b_{bp_float} using the assumed spectral slope of b_{bp} that is specific to each algorithm (Fig. 2). The implications of using an assumed spectral slope within a remote sensing inversion algorithm are reviewed in the discussion. Because the distributions of b_{bp_sat} and b_{bp_float} data are skewed, we calculate basic summary and non-parametric statistics, which include the median and Spearman's rank correlation.

Optics EXPRESS

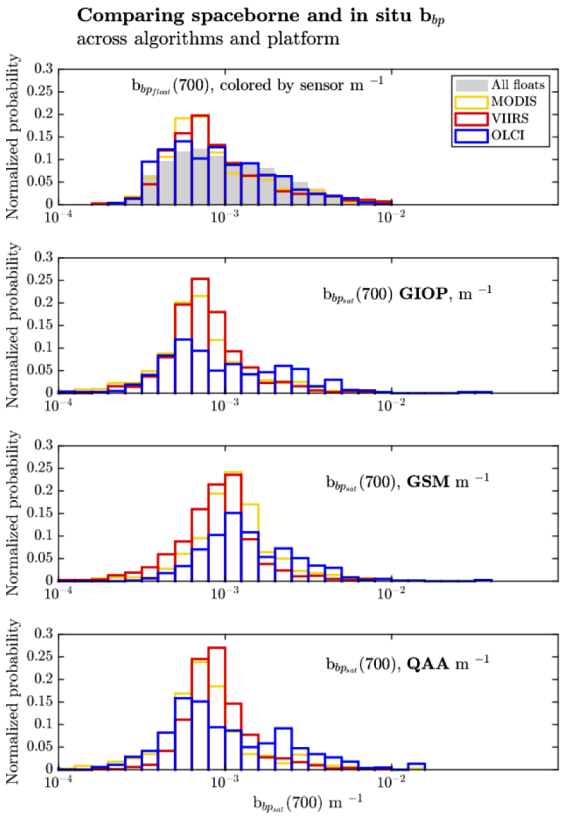

Fig. 2. Comparisons of b_{bp_float} distributions (depending on sensor, top panel), and b_{bp_sat} from the GIOP (2nd panel), GSM (3rd panel) and QAA (4th panel) algorithms across three different sensors (MODIS in yellow, VIIRS in red, OLCI in blue). Grey represents all floats that do not coincide with a satellite observation.

3. Results: b_{bp} matchups and modeled b_{bp} comparisons

There are slightly different matchup statistics between the satellite sensors (Fig. 1) depending on the satellite crossover time and nadir viewing spatial resolution. The probability of a satellite matchup is a strong function of location (Fig. 1). In order for floats to be used for satellite comparisons, they must surface in the daytime during clear sky conditions. The globally integrated effect of this availability is a spatially biased dataset to the Mediterranean and Black Seas. Sixty-three percent of the match-up data are from the Mediterranean and Black Seas, 15% are from the Southern Ocean, 9% are from equatorial regions, 3% are from the North Atlantic, and the rest are from varied locations worldwide. There is no systematic bias depending on the time difference (in hours) between a float and satellite observation (Fig. 3).

Comparisons of b_{bp_float} and b_{bp_sat} are shown for the different sensors across the GIOP, QAA, and GSM algorithms (Fig. 4), with summary statistics in Table 1. Considerable variations in these summary statistics are observed between sensors, algorithms, and regions, with median b_{bp} values differing by more than a factor of two and ranging from 6.2×10^{-4} m^{-1} to 0.0015 m^{-1}. The calculated bias (the median ratio of b_{bp_sat} to b_{bp_float}) between b_{bp_sat} and b_{bp_float} ranges from 0.77 to 1.6, the Median Percent Error (MPE) spans from 27% to 65%, and Spearman's rank correlation coefficients (r) vary from $r = 0.06$ to $r = 0.79$ (Table 1). Despite these seemingly divergent results, several qualitative consistencies are also apparent in the Table 1 statistics. First,

Optics EXPRESS

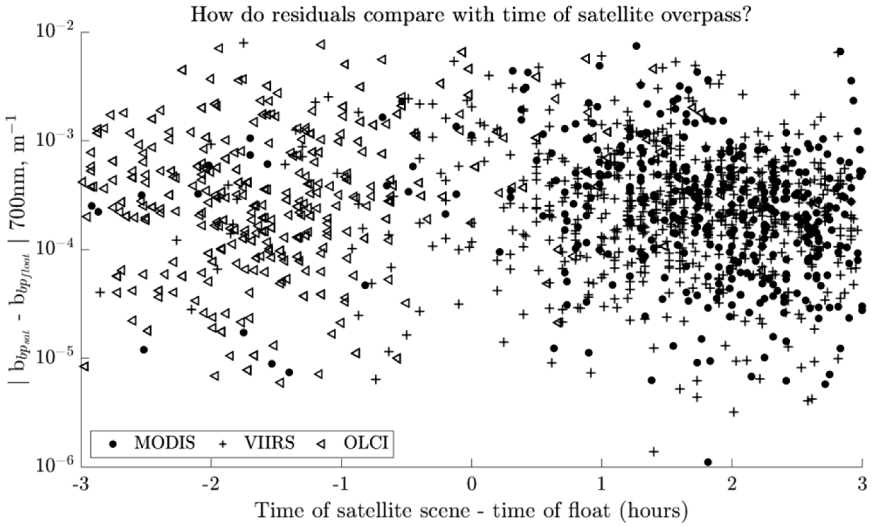

Fig. 3. The absolute value of the difference between b_{bp_sat} and b_{bp_float} is shown against the time (hours) between a satellite overpass and a float observation. The b_{bp_sat} values are shown as an example using the GIOP, but these results are consistent among all algorithms. Satellite data source is indicated by symbol type: filled circle = MODIS, plus sign = VIIRS, and open triangle = OLCI.

the ranking of the median b_{bp_sat} observations from lowest to highest is nearly always GIOP < QAA < GSM, no matter which satellite or region is considered. Second, the Median Percent Error (MPE) is greatest for GSM in all cases and, no matter which sensor or region is considered, GSM (in its standard configuration) always has the lowest 'r' value relative to GIOP or QAA. Finally, b_{bp_sat} derived from MODIS or VIIRS has lower MPE than those derived from OLCI. OLCI has the highest overall number of matchups and MODIS has the fewest, although in the Mediterranean and Black Sea, VIIRS has more matchups than OLCI.

Direct comparisons between b_{bp_sat} and b_{bp_float} in the Mediterranean and Black Seas are confounded by a high degree of scatter (Fig. 4), despite smaller documented variability of either b_{bp_sat} or b_{bp_float} in this region compared to the open ocean (Table 1). This noise limits the degree to which any obvious biases in the b_{bp_sat} comparisons with b_{bp_float} may be identified. When the Mediterranean and Black Sea data are excluded, a different relationship between b_{bp_sat} derived from GIOP, QAA, and GSM and b_{bp_float} is observed. In particular, at low b_{bp_float} values (< 0.001 m^{-1}) GSM greatly overestimates b_{bp_float} and GIOP and QAA do so to a lesser extent. At higher b_{bp_float} values (> 0.005 m^{-1}), GIOP and QAA slightly underestimate b_{bp_float} and there is negligible bias using GSM.

The performance of b_{bp_sat} compared to global observations of b_{bp_float} is a strong function of which algorithm or sensor is used. We found that GIOP and QAA performed better than GSM in oligotrophic regions, especially in waters with b_{bp} (700 nm) < 0.001 m^{-1}, but in waters with higher b_{bp} all three algorithms performed similarly. This finding is consistent with other studies that have shown good agreement when comparing GSM to either in situ or lidar based observations of b_{bp} in waters of moderate to high b_{bp} [31]. In general, the MPEs reported in this study for QAA are larger (by a factor of 3) than those that have been achieved using in situ observations of b_{bp} and shipboard observations of R_{rs} within the QAA framework [12]. A recently published inversion algorithm ([15], hereafter 'LS2') yielded an MPE of 36% when calculated using LS2-derived backscattering from satellite R_{rs} at 670 nm and in situ b_{bp} (n = 25 matchup observations). The magnitude of this MPE is consistent with our reported MPEs from

Optics EXPRESS

Table 1. Matchup summary statistics and non-parametric indices for the 3 satellite sensors and remote sensing inversion algorithms used in this study. Bias is calculated as the median ratio of the satellite values to the float observations, and median percent error (MPE) is calculated as the median of 100% x $|(b_{bp\_sat}/b_{bp\_float} - 1)|$. The 14th and 86th percentiles are reported as estimates of +/- one standard deviation. 'r' is Spearman's rank correlation. Bias, MPE, and r are unitless; b_{bp} (700 nm) and the reported quantiles are m^{-1}.

	b_{bp} (700 nm) source	b_{bp} (700 nm): median m^{-1}	[0.16, 0.84] percentiles, m^{-1}	Bias	MPE (%)	r
GLOBAL SUMMARY STATISTICS – All regions except for the Mediterranean and Black Seas						
MODIS (n = 138)	*Float matches*	0.0012	[0.005, 0.0029]	-	-	-
	GIOP	8.5×10^{-4}	$[6.0 \times 10^{-4}, 0.0018]$	0.80	27	0.79
	GSM	0.0014	[0.001, 0.0024]	1.14	37	0.60
	QAA	8.5×10^{-4}	$[5.0 \times 10^{-4}, 0.0018]$	0.77	28	0.76
VIIRS (n = 192)	*Float matches*	0.0013	$[5.0 \times 10^{-4}, 0.0027]$	-	-	-
	GIOP	9.5×10^{-4}	$[5.0 \times 10^{-4}, 0.0018]$	0.80	33	0.38
	GSM	0.0011	$[6.0 \times 10^{-4}, 0.0019]$	0.80	43	0.21
	QAA	0.0010	$[6.0 \times 10^{-4}, 0.0020]$	0.88	31	0.37
OLCI (n = 537)	*Float matches*	8.5×10^{-4}	$[4.0 \times 10^{-4}, 0.0018]$	-	-	-
	GIOP	0.0011	$[5.0 \times 10^{-4}, 0.0025]$	1.07	45	0.47
	GSM	0.0015	$[9.0 \times 10^{-4}, 0.0028]$	1.6	62	0.32
	QAA	0.0012	$[5.0 \times 10^{-4}, 0.0026]$	1.2	51	0.45
Mediterranean and Black Seas						
MODIS (n = 401)	*Float matches*	6.9×10^{-4}	$[5.0 \times 10^{-4}, 0.0013]$	-	-	-
	GIOP	6.3×10^{-4}	$[4.0 \times 10^{-4}, 0.001]$	0.90	30	0.37
	GSM	0.0010	$[7.0 \times 10^{-4}, 0.0014]$	1.45	65	0.11
	QAA	6.9×10^{-4}	$[4.0 \times 10^{-4}, 0.001]$	0.98	32	0.30
VIIRS (n = 648)	*Float matches*	8.0×10^{-4}	$[5.0 \times 10^{-4}, 0.0013]$	-	-	-
	GIOP	6.2×10^{-4}	$[4.3 \times 10^{-4}, 8.7 \times 10^{-4}]$	0.82	32	0.30
	GSM	8.3×10^{-4}	$[5.0 \times 10^{-4}, 0.0012]$	1.12	46	0.06
	QAA	8.3×10^{-4}	$[6.0 \times 10^{-4}, 0.0011]$	1.12	36	0.29
OLCI (n = 570)	*Float matches*	9.6×10^{-4}	$[5.0 \times 10^{-4}, 0.0020]$	-	-	-
	GIOP	7.5×10^{-4}	$[4.0 \times 10^{-4}, 0.0018]$	0.77	45	0.21
	GSM	0.0012	$[7.0 \times 10^{-4}, 0.0022]$	1.33	65	0.06
	QAA	8.3×10^{-4}	$[5.0 \times 10^{-4}, 0.0019]$	0.90	47	0.21

Optics EXPRESS

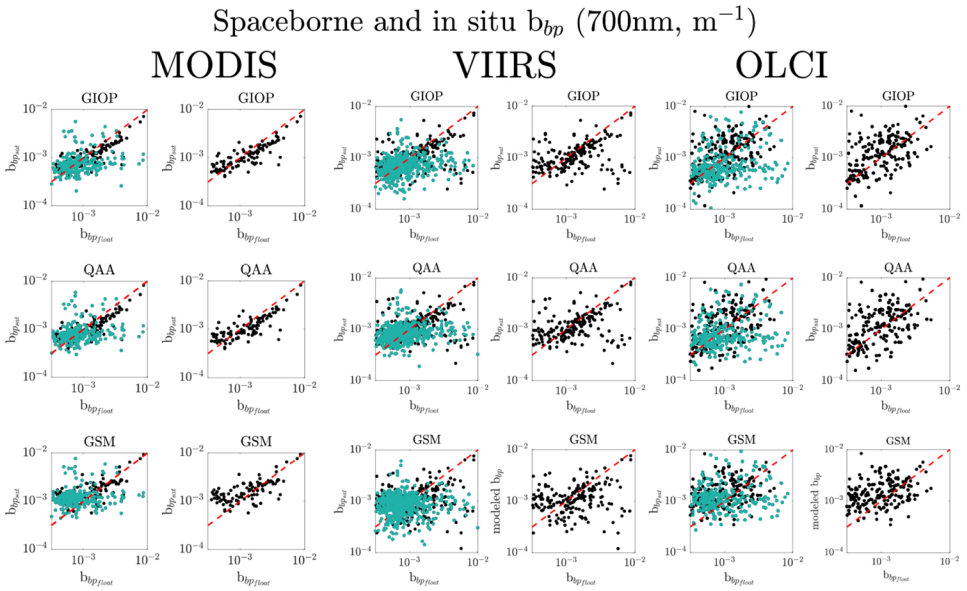

Fig. 4. b_{bp_sat} vs b_{bp_float} matchups for the GIOP, QAA, and GSM inversion algorithms using remote sensing reflectance from MODIS, VIIRS, or OLCI. For each algorithm, the left panel shows all data locations and the right panel shows all locations except the Mediterranean and Black Seas. The Mediterranean and Black Seas data are highlighted in blue in the left panel for each satellite. b_{bp} is at 700 nm m^{-1}. The red dashed line is the 1:1 line.

MODIS and VIIRS using GIOP or QAA, and it reflects the degraded algorithm performance when using satellite rather than in situ R_{rs} as inputs.

There are only 9 float observations common to all three sensors in space and time. This limits the degree to which differences in b_{bp_sat} and b_{bp_float} may be attributed to sensor specifications (e.g., differing signal to noise ratios) or to variability arising from additional float observations. However, if we assume that the underlying distributions of b_{bp_sat} for any given satellite are unbiased with respect to sampling, we can test for statistically significant differences between sensors. This assumption requires that all sensors contain observations from common regions although not precisely at the same time, they have similar proportions of the Southern, Mediterranean and Black seas compared to all data, and they all sample the Pacific and Atlantic basins.

We first tested the statistical differences in the different b_{bp_float} matchup distributions for each sensor to ensure the above assumption is valid. The b_{bp_float} distribution of values at OLCI matchups is statistically different from either MODIS or VIIRS. There are statistically significant differences (at the 5% significance level using a two-sample Kolmogorov-Smirnov test, $p < 1.0 \times 10^{-5}$ in all cases) in the distributions of GIOP, GSM, and QAA b_{bp} values derived from either OLCI, MODIS, or VIIRS. For example, the b_{bp_sat} values from MODIS, OLCI, and VIIRS using the GIOP algorithm are statistically different from each other. In fact, no two distributions of b_{bp_sat} within any given algorithm are similar, even though they are calculated using the same formulae. On the other hand, when b_{bp_sat} distributions are tested for the GIOP and QAA algorithms, they are indeed statistically similar at the 5% significance level ($p = 0.92$), no matter which sensor is used, for all places except the Mediterranean and Black Seas. This suggests that there is greater similarity in the b_{bp} observations within a given satellite and/or region than among algorithm choice across different sensors.

Optics EXPRESS

4. Discussion

Satellite derived estimates of the particulate backscattering coefficient at 700 nm vary among sensors. No matter which algorithm is used, we found that b_{bp_sat} correlations are highest in open ocean waters with MODIS (r = 0.60 to 0.79) compared to VIIRS (r = 0.21 to 0.38) and OLCI (r = 0.32 to 0.47) because R_{rs} observations are noisiest using either VIIRS or OLCI, on the basis of their coefficient of variations within the 5×5-pixel box, and on their relatively higher MPEs. The original Bailey and Werdell criteria stipulate that the median coefficient of variation in R_{rs} around a 5×5-pixel box be less than 15%. Although we found that all three sensor data sets have median coefficients of variation less than 15% for any location and time, VIIRS and OLCI have higher average coefficients of variation (8% and 30%, respectively) than MODIS (5%) for all bands between 412 and 555nm, as well as the aerosol optical thickness at 865. The coefficient of variation has a strong dependency on wavelength and surpasses 15% at wavelengths longer than 555nm. This finding suggests a revisit of the Bailey and Werdell criteria, which were originally formulated to leverage the quality of satellite observations with the quantity of in situ matchups. Using a median coefficient of variation in $R_{rs}(\lambda)$ does not reflect the average spatial variability within a particular place and time. Choosing a different metric to quantify spatial heterogeneity, such as the standard deviation in R_{rs} for each wavelength, may be useful so that it can be directly contrasted with the uncertainty expected from the spectrally varying signal-to-noise ratios that are specific for each sensor. The results herein support the use of autonomous floats for performing ocean color validations. Now that the quantity of in situ matchups is less of a limiting factor, more restrictive matchup criteria may be appropriate in future work.

Satellite derived estimates of the particulate backscattering coefficient at 700 nm also vary among algorithm choice. The GIOP, GSM, and QAA algorithms can all be optimized with local datasets, and their spectral shape assumptions of optical properties can be changed with different formulae if desired. We chose to compare them here in their default operational configuration because the products from these three algorithms are widely distributed, and thus it is critical to examine how they may be biased when confronted with a large global dataset. Importantly, their wide distribution does not imply that these are the best inversion algorithms available. If we view the results herein as a sample representation of how well we currently retrieve b_{bp} from satellites, we can outline avenues for improvement in future work.

In the default configuration, the major difference between the GSM and either the GIOP or QAA is the assumed b_{bp} spectral slope. It is critical to evaluate our results in the context of b_{bp} slope because floats provide b_{bp} at 700 nm and ocean color b_{bp} values are typically compared between 440 and 555nm. The GSM assumes a constant b_{bp} spectral slope of -1, whereas the GIOP and QAA allow the b_{bp} spectral slope to vary as a function of R_{rs} ratios, effectively making the b_{bp} slope a function of chlorophyll. In its standard configuration, the GSM overestimates b_{bp} by factors up to 50%, which is a probable consequence of both the constant b_{bp} spectral slope and the Raman scattering correction, which has been shown to introduce large (> 20%) uncertainties in b_{bp} when GSM is used [24]. These findings suggest that caution should be applied when using the GSM algorithm in oligotrophic environments with low b_{bp} because it could result in large overestimates of particulate organic carbon (POC) or phytoplankton biomass when b_{bp} to carbon relationships are used.

One way to avoid uncertainty introduced by the assumption of b_{bp} spectral slope is to employ inversion algorithms that do not require an assumed shape of b_{bp}. This can be done by retrieving the spectral beam attenuation coefficient from ocean color [32] so that b_{bp} may be expressed as the linear difference between particulate beam attenuation (which is a well described function of wavelength) and particulate absorption. The 'LS2' model is a more recent and promising method that updates the Loisel and Stramski (2000) inversion algorithm [27] and independently retrieves b_{bp} at any wavelength knowing R_{rs} and the solar zenith angle. The radiative transfer simulations used to develop this model were extended so that it can be applied in both clear and turbid waters.

Optics EXPRESS

The new model may be of great use for evaluating b_{bp_sat}, especially when there are additional observations from b_{bp_float} in coastal waters.

In order for floats to be reliable sources of data for ocean color validation, they would need to provide backscattering measurements in the green bands, both because the signal to noise ratio in satellite sensors is higher than in the red and the green bands are minimally influenced by absorption by phytoplankton and water. Another consideration when comparing b_{bp_float} to b_{bp_sat} is to correct for surface bubbles and white caps. In this study, we corrected float data for the presence of surface bubbles and other spikes within a vertical profile, which contribute high values of b_{bp} not representative of the average mixed layer value. This processing step does not substantially change the median for the float dataset, but it does decrease the arithmetic mean b_{bp} by 40% because the frequency of values exceeding the 95% quantile value of 0.005 m^{-1} more than halves. If float profiles were not de-spiked, there would be more instances of high b_{bp} values, which would lower the bias for some of the algorithm/sensor pairs considered. At the same time, surface bubbles also affect R_{rs} observations because they appear as bright spots from high scattering. White cap corrections made to R_{rs} values may appear as regional dependencies [33], particularly in areas with high winds. Although it is outside of the scope of this study, future work may benefit from examining potential sources of bias from white caps.

In this study we ask, 'Can autonomous floats be used to evaluate satellite estimates of particulate backscatter in the open ocean?' Backscattering sensors on autonomous floats provide a rich in situ data set (compared to historical ship-based observations) for evaluating the performance of b_{bp_sat} from ocean color inversion algorithms. The generally long deployment duration of floats, their relatively high temporal resolution profiling, and their availability to be compared across multiple satellite sensors significantly improve successful match-up observations with satellite overpasses. Despite these major advances, the spatial coverage of float observations remains sparse and regionally biased when considered at the full global scale (Fig. 1). This current shortcoming limits our ability to fully evaluate spatial-temporal biases in inversion algorithm b_{bp} products and, consequently, to begin investigating parameter improvements to address these biases. Clearly, a continued effort to increase the global distribution of these important autonomous measurements is warranted, as well as investigation of other independent sources of b_{bp} measurements for improving the coverage of ocean color match-up data.

A. Appendix

A.1. Description of R_{rs} inversion algorithms

The remotely sensed retrieval of b_{bp} is an inverse problem requiring a forward model that describes the relationship between R_{rs} and b_{bp}. There are several inversion algorithms available to determine b_{bp}, and we consider the three algorithms currently distributed via NASA ocean color processing: the Generalized Inherent Optical Property model (GIOP, [28]), the Garver-Siegel-Maritorena algorithm (GSM, [29]), and the Quasi Analytical Algorithm (QAA, [30]). The general architecture of these algorithms is similar but they differ in their assumed spectral shapes of IOPs; Full details are available in the references for each algorithm but we provide a brief description below. In all cases, above water remote sensing reflectance (R_{rs}) is propagated across the air-water interface into r_{rs} using the approximation from [30] below:

$$r_{rs}(\lambda) = \frac{R_{rs}(\lambda)}{0.52 + 1.7R_{rs}(\lambda)} \tag{3}$$

The relationship between r_{rs} and inherent optical properties can be expressed using the formulation in [34]:

$$r_{rs}(\lambda) = \sum_{i=1}^{2} G_i^{*}[u(\lambda)]^i \tag{4}$$

Optics EXPRESS

where $G_1 = 0.0949$ and $G_2 = 0.0794$ for use in the GIOP and GSM model. The method in [30] uses $G_1 = 0.0985$ and $G_2 = 0.1247$ within the QAA to leverage the coefficients that work best for highly scattering coastal waters and lower scattering oligotrophic seas.

$u(\lambda)$ is given by the ratio of backscattering (b_b) to the sum of absorption (a) and backscattering (b_b), or

$$u(\lambda) = \frac{b_b(\lambda)}{a(\lambda) + b_b(\lambda)} \tag{5}$$

Determining b_{bp} from Eq. (3) is carried out in different ways depending on the inversion algorithm used. The GIOP determines b_{bp} by solving for the combination of IOPS that produce the lowest misfit between reconstructed r_{rs} and observed r_{rs}. To accomplish this, $a(\lambda)$ and $b_b(\lambda)$ are expressed as the sum of their parts:

$$a(\lambda) = a_w(\lambda) + M_{dg}a^*_{dg}(\lambda) + M_{ph}a^*_{ph}(\lambda) \tag{6}$$

$$b_b(\lambda) = b_{bw}(\lambda) + M_{bp}b^*_{bp}(\lambda) \tag{7}$$

Where a_w and b_{bw} are absorption and scattering by pure water (respectively) and M denotes the eigenvalues that modify its eigenvector (a* or b*) for CDOM and non-algal particles (collectively dg), phytoplankton (ph), and all particles (p). In the GIOP default configuration,

$$a^*_{dg}(\lambda) = e^{-S_{dg}} \tag{8}$$

where $S = 0.018\ nm^{-1}$ and is spectrally independent. $a^*_{ph}(\lambda)$ is determined from satellite estimates of chlorophyll a, normalized to $0.055\ m^2\ mg^{-1}$. The spectral shape of b_{bp} is given by

$$b_{bp}(\lambda) = b_{bp}(\lambda_0)(\lambda/\lambda_0)^{-\gamma} \tag{9}$$

where γ is an empirically derived function using blue to green band ratios of r_{rs}, which effectively makes γ a function of chlorophyll. The three unknown eigenvalues are solved, and b_{bp} is thus determined, using the Levenberg-Marquardt least squares method to invert observed r_{rs}.

In contrast to the GIOP, the QAA determines $a(\lambda)$ using empirically derived R_{rs} or r_{rs} band ratios (depending on the R_{rs} (670nm) value) in combination with the known spectral shape of absorption by pure water [35]. Then, because $\mu(\lambda)$ and $a(\lambda)$ are known, b_b is solved analytically using Eq. (5), and b_{bp} is retrieved after subtracting scattering by pure water [36]. The assumed slope of the backscattering spectrum is calculated as in the GIOP. The updated QAA (v6) is used in this study, with more details available at <<http://www.ioccg.org/groups/Software_OCA/QAA_v6_2014209.pdf>>.

While the GIOP and QAA allow the shape of b_{bp} to vary, the GSM inversion model is a semi-analytical model that, in its default configuration, holds the spectral shape of IOPs constant and solves for chl a concentration, the cdm absorption coefficient (a_{dg}), and the backscatter coefficient (b_{bp}).

The governing equations are below:

$$a^*_{ph}(\lambda) = Chl^* a_{ph}(\lambda) \tag{10}$$

$$a^*_{dg}(\lambda) = a_{dg}(\lambda_0)^*\, e^{-S_{dg}(\lambda - \lambda_0)} \tag{11}$$

$$b^*_{bp}(\lambda) = b_{bp}(\lambda_0)(\lambda/\lambda_0)^{-\gamma} \tag{12}$$

where a^*_{ph} is the chl a specific absorption coefficient, S is held constant to 0.02, and the backscatter coefficient (γ) is held to 1). The procedure used to derive default configuration parameters is simulated annealing, which allows parameter searches in the direction of lower

Optics EXPRESS

model performance, so it is little influenced by nearly performance maximums and instead gives solutions that represent that best model performance over a large search range.

The wavelengths used in the inversions are specific to each sensor. For MODIS R_{rs}, 412, 443, 488, 531, 555, 667 nm are used. For VIRIS R_{rs}, 410, 443, 485, 551, and 671 nm are used. For OLCI R_{rs}, 412, 442, 490, 510, 560, and 665 nm are used.

Funding

National Aeronautics and Space Administration (80NSSC18K0957, NNX15AAF30G).

Acknowledgments

We gratefully acknowledge Nils Haentjens for assistance with NASA level-2 ocean color imagery, Sasha Kramer for editorial assistance, and Jeremy Werdell for useful and supportive discussions. We thank Giorgio Dall'Olmo, Hubert Loisel, and Dariusz Stramski for comments that greatly enhanced this manuscript. The authors declare that there are no conflicts of interest related to this article. These data were collected and made freely available by the International Argo Program and the national programs that contribute to it (http://doi.org/10.17882/42182). The Argo Program is part of the Global Ocean Observing System.

References

1. D. Stramski, R. A. Reynolds, M. Kahru, and B. G. Mitchell, "Estimation of particulate organic carbon in the ocean from satellite remote sensing," Science **285**(5425), 239–242 (1999).
2. M. J. Behrenfeld, E. Boss, D. A. Siegel, and D. M. Shea, "Carbon-based ocean productivity and phytoplankton physiology from space," Global Biogeochem. Cycles **19**(1), 447 (2005).
3. T. S. Kostadinov, D. A. Siegel, and S. Maritorena, "Retrieval of the particle size distribution from satellite ocean color observations," J. Geophys. Res.: Oceans **114**(C9), C09015 (2009).
4. H. Claustre, J. Bishop, E. Boss, B. Stewart, J.-F. Berthon, C. Coatanoan, K. Johnson, A. Lotiker, O. Ulloa, M.-J. Perry, F. D'Ortenzio, O. Hembise Fanton D'Andon, and J. Uitz, "Bio-optical profiling floats as new observational tools for biogeochemical and ecosystem studies," In: J. Hall, D.E. Harrison, and D. Stammer, eds. *Proceedings of the "OceanObs'09: Sustained Ocean Observations and Information for Society" Conference*, Venice, Italy, 21-25 September 2009. 2: | DOI: 10.5270/OceanObs09.cwp.17. (2010).
5. E. Boss and M. Behrenfeld, "In situ evaluation of the initiation of the North Atlantic phytoplankton bloom," Geophys. Res. Lett. **37**(18), 79 (2010).
6. E. Organelli, H. Claustre, A. Bricaud, M. Barbieux, J. Uitz, F. D'Ortenzio, and G. Dall'Olmo, "Bio-optical anomalies in the world's oceans: An investigation on the diffuse attenuation coefficients for downward irradiance derived from Biogeochemical Argo float measurements," J. Geophys. Res.: Oceans **122**(5), 3543–3564 (2017).
7. M. Barbieux, J. Uitz, A. Bricaud, E. Organelli, A. Poteau, C. Schmechtig, B. Gentili, G. Obolensky, E. Leymarie, C. Penkerc'h, and F. D'Ortenzio, "Assessing the Variability in the Relationship Between the Particulate Backscattering Coefficient and the Chlorophyll a Concentration From a Global Biogeochemical-Argo Database," J. Geophys. Res.: Oceans **123**(2), 1229–1250 (2018).
8. A. Mignot, R. Ferrari, and H Claustre, "Floats with bio-optical sensors reveal what processes trigger the North Atlantic bloom," Nat. Commun. **9**(1), 190 (2018).
9. N. Haëntjens, E. Boss, and L. D. Talley, "Revisiting Ocean Color algorithms for chlorophyll a and particulate organic carbon in the Southern Ocean using biogeochemical floats," J. Geophys. Res.: Oceans **122**(8), 6583–6593 (2017).
10. A. Poteau, E. Boss, and H. Claustre, "Particulate concentration and seasonal dynamics in the mesopelagic ocean based on the backscattering coefficient measured with Biogeochemical-Argo floats," Geophys. Res. Lett. **44**(13), 6933–6939 (2017).
11. H. Claustre French National Centre for Scientific Research. Laboratoire d'Océanographie de Villefranche, France. (personal communication, 2017).
12. G. Zheng, D. Stramski, and R. A. Reynolds, "Evaluation of the Quasi-Analytical Algorithm for estimating the inherent optical properties of seawater from ocean color: Comparison of Arctic and lower-latitude waters," Remote Sens. Environ. **155**, 194–209 (2014).
13. D. Stramski, R. A. Reynolds, M. Babin, S. Kaczmarek, M. R. Lewis, R. Röttgers, and H. Claustre, "Relationships between the surface concentration of particulate organic carbon and optical properties in the eastern South Pacific and eastern Atlantic Oceans," Biogeosciences **5**(1), 171–201 (2008).
14. E. Boss, D. Swift, L. Taylor, P. Brickley, R. Zaneveld, S. Riser, and P. G. Strutton, "Observations of pigment and particle distributions in the western North Atlantic from an autonomous float and ocean color satellite," Limnol. Oceanogr. **53**(5part2), 2112–2122 (2008).

Optics EXPRESS

15. H. Loisel, D. Stramski, D. Dessailly, C. Jamet, L. Li, and R. A. Reynolds, "An inverse model for estimating the optical absorption and backscattering coefficients of seawater from remote-sensing reflectance over a broad range of oceanic and coastal marine environments," J. Geophys. Res.: Oceans **123**(3), 2141–2171 (2018).
16. Bittig Henry, Wong Annie, and Plant Josh, Coriolis Argo Data Management Team. "BGC-Argo synthetic profile file processing and format on Coriolis GDAC," https://doi.org/10.13155/55637. (2018).
17. A. Barnard Sea-Bird Scientific, Bellevue, Washington, USA. (personal communication, 2017).
18. Annie Wong and Robert Keeley, Thierry Carval and the Argo Data Management Team "Argo Quality Control Manual for CTD and Trajectory Data," http://dx.doi.org/10.13155/33951. (2019).
19. C. de Boyer Montégut, G. Madec, A. S. Fischer, A. Lazar, and D. Iudicone, "Mixed layer depth over the global ocean: An examination of profile data and a profile-based climatology," J. Geophys. Res.: Oceans **109**(C12), C12003 (2004).
20. D. Stramski, E. Boss, D. Bogucki, and K. J. Voss, "The role of seawater constituents in light backscattering in the ocean," Prog. Oceanogr. **61**(1), 27–56 (2004).
21. S. W. Bailey and P. J. Werdell, "A multi-sensor approach for the on-orbit validation of ocean color satellite data products," Remote Sens. Environ. **102**(1-2), 12–23 (2006).
22. R. H. Stavn and A. D. Weidemann, "Optical modeling of clear ocean light fields: Raman scattering effects," Appl. Opt. **27**(19), 4002–4011 (1988).
23. H. R. Gordon, "Contribution of Raman scattering to water-leaving radiance: a reexamination," Appl. Opt. **38**(15), 3166–3174 (1999).
24. T. K. Westberry, E. Boss, and Z. Lee, "Influence of Raman scattering on ocean color inversion models," Appl. Opt. **52**(22), 5552–5561 (2013).
25. Z. Lee, C. Hu, S. Shang, K. Du, M. Lewis, R. Arnone, and R. Brewin, "Penetration of UV-visible solar radiation in the global oceans: Insights from ocean color remote sensing," J. Geophys. Res.: Oceans **118**(9), 4241–4255 (2013).
26. L. I. McKinna, P. J. Werdell, and C. W. Proctor, "Implementation of an analytical Raman scattering correction for satellite ocean-color processing," Opt. Express **24**(14), A1123–A1137 (2016).
27. H. Loisel and D. Stramski, "Estimation of the inherent optical properties of natural waters from the irradiance attenuation coefficient and reflectance in the presence of Raman scattering," Appl. Opt. **39**(18), 3001–3011 (2000).
28. P. J. Werdell, B. A. Franz, S. W. Bailey, G. C. Feldman, E. Boss, V. E. Brando, M. Dowell, T. Hirata, S. J. Lavender, Z. Lee, and H. Loisel, "Generalized ocean color inversion model for retrieving marine inherent optical properties," Appl. Opt. **52**(10), 2019–2037 (2013).
29. S. Maritorena, D. A. Siegel, and A. R. Peterson, "Optimization of a semianalytical ocean color model for global-scale applications," Appl. Opt. **41**(15), 2705–2714 (2002).
30. Z. Lee, K. L. Carder, and R. A. Arnone, "Deriving inherent optical properties from water color: a multiband quasi-analytical algorithm for optically deep waters," Appl. Opt. **41**(27), 5755–5772 (2002).
31. M. J. Behrenfeld, Y. Hu, C. A. Hostetler, G. Dall'Olmo, S. D. Rodier, J. W. Hair, and C. R. Trepte, "Space-based lidar measurements of global ocean carbon stocks," Geophys. Res. Lett. **40**(16), 4355–4360 (2013).
32. C. S. Roesler and E. Boss, "Spectral beam attenuation coefficient retrieved from ocean color inversion," Geophys. Res. Lett. **30**(9), 1468 (2003).
33. H. M. Dierssen, "Hyperspectral measurements, parameterizations, and atmospheric correction of whitecaps and foam from visible to shortwave infrared for ocean color remote sensing," Front. Earth Sci. **7**, 14 (2019).
34. H. R. Gordon, O. B. Brown, R. H. Evans, J. W. Brown, R. C. Smith, K. S. Baker, and D. K. Clark, "A semianalytic radiance model of ocean color," J. Geophys. Res.: Atmos. **93**(D9), 10909–10924 (1988).
35. R. M. Pope and E. S. Fry, "Absorption spectrum (380–700 nm) of pure water. II. Integrating cavity measurements," Appl. Opt. **36**(33), 8710–8723 (1997).
36. X. Zhang, L. Hu, and M. X. He, "Scattering by pure seawater: effect of salinity," Opt. Express **17**(7), 5698–5710 (2009).